Theor Chem Acc (2011) 130:463–473
DOI 10.1007/s00214-011-1024-7

REGULAR ARTICLE

Facial dissociations of water molecules on the outside and inside of armchair single-walled silicon nanotubes: theoretical predictions from multilayer quantum chemical calculations

Yong Wang · Guoyong Fang · Jing Ma · Yuansheng Jiang

Received: 7 March 2011 / Accepted: 13 August 2011 / Published online: 28 August 2011

Abstract The possible reaction pathways of dissociative adsorption of a single water molecule on the sidewalls of armchair (n, n) (n = 4–10) single-walled silicon nanotubes (SWSiNT) have been investigated by the multilayer models. Both the simplified fragment embedding and ONIOM calculations were carried out to study the diameter dependence of reactivity for the dissociation of water on SWSiNTs. The active fragments with different cluster sizes, such as $Si_{16}H_{10}$, $Si_{30}H_{16}$, and $Si_{10m}H_{4m}$ (m = 4–10), were used for the multilayer calculations. The employment of the medium-sized $Si_{30}H_{16}$ cluster is able to reach a good balance between the computational efficiency and accuracy for the large-sized reaction system. In comparison with those full B3LYP/LANL2DZ calculations for Si(4,4) and Si(5,5) nanotubes, the approximate multilayered models can give reasonable predictions on the optimized geometries, activation energies, and exothermic energies with significant reduction in computational cost. The external complexes of the dissociative adsorption of H_2O on SWSiNTs were predicted to be more stable than those internal complexes. The convex surfaces of SWSiNTs were also more reactive to H_2O with the smaller activation barrier energies (10–13 kcal/mol) than those (15–22 kcal/mol) on the concave side. Both the activation barriers and exothermic energies of dissociative adsorptions of H_2O on the internal (external) sidewalls of armchair SWSiNT were found to be insensitive to the tube curvature. The passivation of the outer surface and the removal of water molecules may be crucial for the experimental preparation of the single-walled silicon nanotubes.

Keywords Single-walled silicon nanotube · Armchair · Reactivity · Curvature dependence · ONIOM · Fragment embedding model

1 Introduction

Single-walled carbon nanotubes (SWCNTs) can be viewed as a strip cut from an infinite graphene sheet and rolled up to form a tube. Shortly after multi-walled carbon nanotubes initially observed by Iijima in 1991 [1], the chemistry of SWCNTs has attracted both experimental and theoretical interests. SWCNTs exhibit interesting electronic, mechanical, and structural properties and potential applications to chemical sensors and nanometer-scale electronic devices, etc. Characterized with the diversity of tube diameters and chiral angles, SWCNTs have higher curvature-induced chemical reactivity than the flat graphite [2, 3]. Chemical compounds could be added to the internal and external sidewalls of the nanotubes [4–9].

Belonging to the same group IV as carbon element, silicon shows some similarities in the formation of covalent

Dedicated to Professor Shigeru Nagase on the occasion of his 65th birthday and published as part of the Nagase Festschrift Issue.

Electronic supplementary material The online version of this article (doi:10.1007/s00214-011-1024-7) contains supplementary material, which is available to authorized users.

Y. Wang · G. Fang · J. Ma (✉) · Y. Jiang
Key Laboratory of Mesoscopic Chemistry of MOE,
School of Chemistry and Chemical Engineering,
Institute of Theoretical and Computational Chemistry,
Nanjing University, Nanjing 210093,
People's Republic of China
e-mail: majing@nju.edu.cn

Y. Wang
College of Chemistry, Chemical Engineering and Material Science, Soochow University, Su Zhou 215123,
People's Republic of China

σ bonds in sp^3 hybridization mode but distinct difference in the strength of π bonds formed through sp^2 hybridization. The rather weak and reactive Si=Si bond has brought about a rich chemistry, arousing intensive interest in the design, synthesis, and characterization of unsaturated silicon-containing compounds [10–19]. There has also been a surge of interest to build various silicon nanostructures, because of their apparent compatibility with the silicon-based microelectronics [20–42]. Although Yang and coworks [43] have reported multi-walled silicon nanotubes prepared by chemical vapor deposition (CVD) process on Al_2O_3 substrate, the actual SWSiNT based on the rolled up sp^2 graphene-like sheet has not been found yet (probably due to the preference for sp^3 hybridization structures).

The long-standing dream of preparing sp^2 SiNT also triggered many theoretical studies on the electronic structures and properties of some possible SWSiNTs [40, 44–58]. A systematic comparison between SiNTs and CNTs was made by Fagan et al. using density functional theory (DFT) calculations [44, 45]. Through tight-binding molecular dynamics simulations, Andriotis et al. demonstrated that the encapsulation of metals such as Ni and V could stabilize SWSiNTs [47]. Zhang et al. [48] predicted that SWSiNTs prefer armchair to zigzag structures by using DFT with the three-parameter hybrid functional (B3LYP). In addition, Zhang and coworkers [40] found that SiNTs could adopt a number of distorted tubular structures via density functional tight-binding molecular dynamics simulations and quantum chemical methods (Hatree-Fock (HF) and B3LYP). Silicon nanotubes in zigzag, armchair, and chiral configurations were predicted to be semiconductors, with evident curvature dependence of stability and band structure [46]. Pradhan and Ray [51] also pointed out that SiNTs do not appear to be metallic in armchair configurations. Almost all those theoretical studies were concentrated on the relative stability of the SiNTs [46–52], but the chemical reactivity of SWSiNTs has still been less explored yet.

Unlike the relatively inert carbon nanotubes, the weak silicon–silicon bonds may make SWSiNTs reactive even toward the attachment of ambient gases such as water molecules. Theoretical calculations demonstrated that water molecules took a physical absorption on CNT with small binding energy of less than 1 kcal/mol [59], only the geometry defects on carbon substrates rendered them feasible to dissociate water molecules with activation barriers of about 16–55 kcal/mol [60], It is hence interesting to know how a water molecule behaves when it attacks the outer or inner surface of SiNTs. *Is the sidewall of SWSiNT reactive enough to dissociate the attached water molecules at a mild condition?*

We attempt to answer this question in the present work through a systematic study on the possible reaction pathways of water on sidewalls of SWSiNTs as a function of tube diameter (Scheme 1). In order to reduce the formidable computational costs of direct quantum mechanics (QM) calculations on a realistic nanotube model, we resort to some simplified multilayer models. Being designed for the study of the reaction mechanism on solid surfaces, there are several kinds of multilayer surface models, almost following the same philosophy of dividing the complex system into two subsystems and treating the active fragment at a relatively high theoretical level and the other substrate (that distant from reaction center) at a lower level. The difference in various multilayer models mainly lies in the different way of describing the boundary between the high and low levels. By modeling the inactive part by the inexpensive molecular mechanics (MM) potentials, the hybrid quantum mechanics/molecular mechanics (QM/MM) scheme, which was originally proposed by Warshel and Levitt [61], saves computational efforts to a large degree and gains great popularity in predicting properties and reactions of complex systems. QM/MM methods usually consider the influence of the MM region on the QM calculation of active unit by using the electrostatics

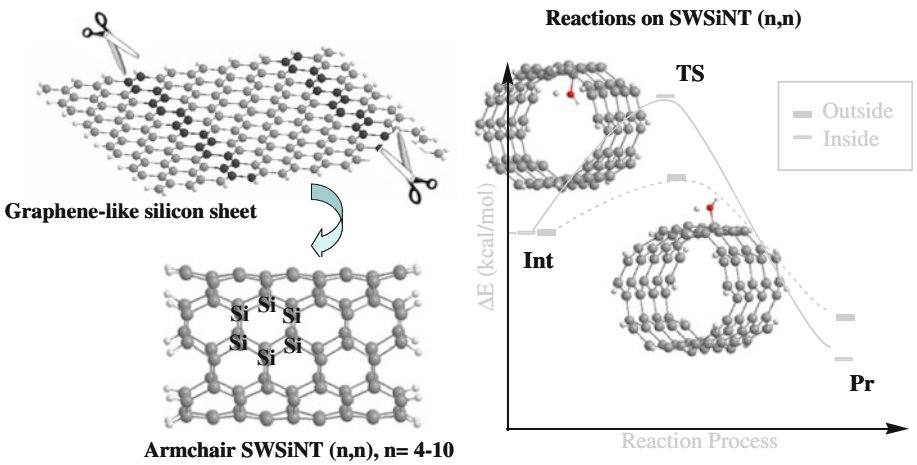

Scheme 1 Illustration of single-walled silicon nanotube (SWSiNT) and its reactions toward the attachment of a single water molecule on outside or inside surfaces

embedding model and proper description of dangling bonds at boundary. The integrated molecular orbital molecular mechanics (IMOMM) approach, proposed by Maseras and Morokuma, provided a physically appealing way to introduce MM corrections in full geometry optimizations for the target systems [62]. The IMOMM method was further modified specifically for optimization of surfaces, called surface integrated molecular orbital molecular mechanics (SIMOMM) method [63]. It was shown that SIMOMM is approximately 100 times faster than the full QM calculations on the large Si(100) surface models [63]. In recent years, the multilayered ONIOM models, which contain a hierarchy of different theoretical levels of ab inito or semiempirical quantum chemical models, have become increasingly popular in understanding reaction mechanisms of complicated systems.

In fact, the widely applied multilayer models for surface reactions can find their root in the early cluster embedding models [64–68], which considered the locality of the adsorbate–substrate bonding interactions as well as the boundary effects that connecting the "reactive" cluster and the underlying "unperturbed" substrate. For studying chemisorption and surface reactions, more sophisticated considerations of the boundary effect have been introduced in the dipped adcluster model (DAM) by involving the metal-admolecule electron transfer and the image force correction [69, 70].

Herein, the dissociative adsorptions of H_2O on the external and internal sidewalls of (n, n) armchair SWSiNTs (abbreviated as Si(n, n), $n = 4$–10) are investigated by using several two-layered calculation schemes, including the simplified fragment embedding and ONIOM models. To validate the performance of the approximate multilayer QM models, the full QM calculations are also carried out on Si(4,4) and Si(5,5) tubes with small tube diameters. Through increasing the tube diameters from Si(4,4) to Si(10,10), we will show the curvature dependence in kinetic stability of SWSiNTs in ambient water and the relative reactivity of H_2O with two sidewalls, outside versus inside, of armchair silicon nanotubes.

2 Surface models and computational details

The selected embedding surface models and the computational details of QM and ONIOM optimizations are given below.

2.1 Simplified fragment embedding model

The studied (n, n) armchair SWSiNT consists of nine silicon layers, with the dangling bonds at two edges terminated by hydrogen atoms. In order to save the computational costs in our systematic study of reactions outside and inside the SWSiNTs (that ranging from (4,4) to (10,10) tubes), we adopt the two-layered fragmentation QM calculations. As shown in Fig. 1, we separate the SWSiNT into two parts, the active region and the inactive substrate. In reality, the active and inactive subsystems can be treated at either the same theoretical level or different levels. Here, we use the two different theoretical levels: the higher-level calculation with B3LYP/6-31G* is carried out on the active part, while B3LYP with the effective core potential, LANL2DZ, is employed as a lower theoretical level. In our simplified embedding models, we mainly consider the geometry fitness at the border between the active fragment and the remaining substrate. In the first step, the whole reaction system (including water molecule and Si (n, n) tube) is optimized at the level of B3LYP/LANL2DZ. Then, the reactive site is cut from the B3LYP/LANL2DZ optimized structure, in which the dangling bonds of reactive site are saturated by H atoms. The coordinates of these H atoms are fixed at the geometry of the replaced Si atoms in substrate during the optimization of reactive fragment at the higher level of B3LYP/6-31G*. The obtained energy for the reactive part is labeled as E_{reactive}. The newly obtained atomic coordinates in reactive site at higher level are further embedded into the optimized geometry of the whole reaction system. Finally, a single-point energy calculation at lower theoretical level is performed on the bulk system embedded with the active fragment. The energy of the whole reaction system containing both the adsorbate and substrate is then called E_{bulk}.

The boundary effects and convergence with increasing size of active fragment are crucial to the performance of the embedded fragment models. To test the size effect of the active fragments on the optimized geometry and activation barriers, we select three different models with the increasingly larger clusters of $Si_{16}H_{10}$ (Cluster I), $Si_{30}H_{16}$ (Cluster II), and $Si_{10m}H_{4m}$ (Cluster III, where $m = 4$–10, e.g., $Si_{100}H_{40}$ fragment used for Si(10,10) nanotube), as shown in Fig. 1. The frequency tests are more computationally expensive than the geometry optimizations, so that the B3LYP/6-31G* frequency calculations are only available for the fragment models of Cluster I: $Si_{16}H_{10}$ and Cluster II: $Si_{30}H_{16}$. In order to better describe the dissociative adsorption of H_2O on the external and internal sidewalls of SWSiNT, the single-point energy calculations at even higher basis set level of B3LYP/6-311+G (d, p) are performed on the B3LYP/6-31G* optimized structures, designated by the standard notation of B3LYP/6-311+G (d, p)//B3LYP/6-31G* (Table S1 of Supporting Information).

The exothermic energies, E_{exo}, of adsorption of a single water molecule on SWSiNT sidewalls can be calculated

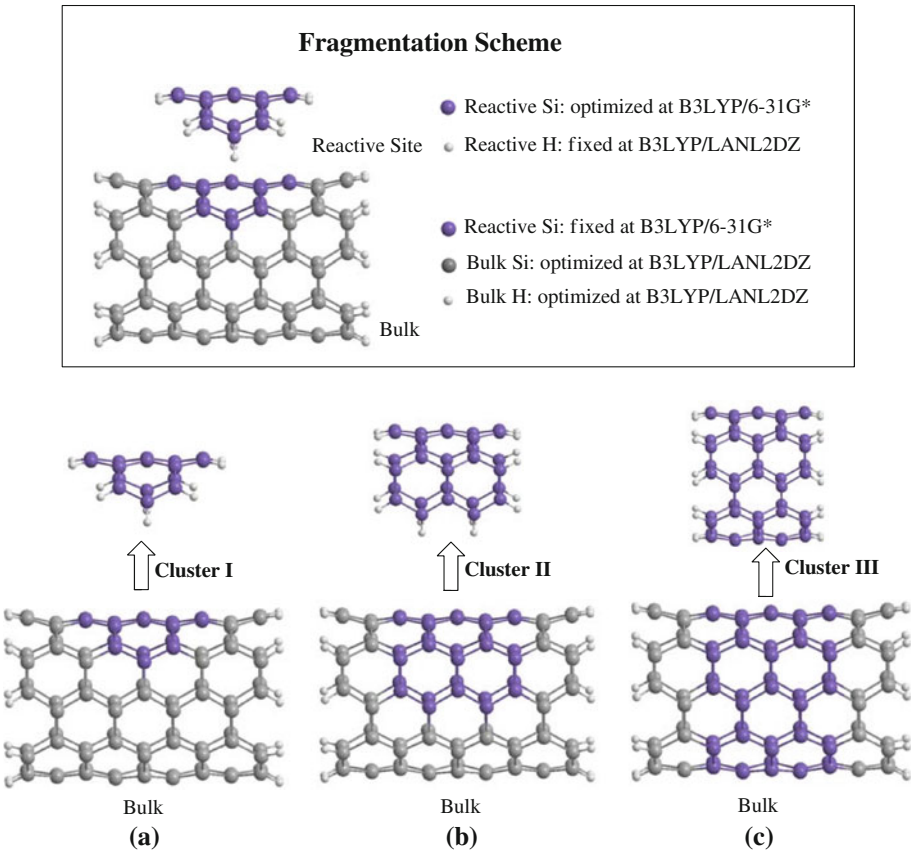

Fig. 1 Partition scheme used in multilayered fragment embedding models: **a** Cluster I: $Si_{16}H_{10}$, **b** Cluster II: $Si_{30}H_{16}$, and **c** Cluster III: $Si_{50}H_{20}$

from the energy difference between the product, E_{product}, and reactants, $E_{\text{reactants}}$.

$$E_{\text{exo}} = E_{\text{product}} - E_{\text{reactants}} \tag{1}$$

To cut down the computational costs for such large systems of reactions on nanotubes, the simplified fragment embedding model is used to estimate the energies of reactants and products.

$$E_{\text{product}} = E_{\text{reactive}}^{\text{product}} + E_{\text{bulk}}^{\text{product}} + \Delta E_{\text{interaction}}^{\text{product}} \tag{2}$$

$$E_{\text{reactants}} = E_{\text{reactive}}^{\text{reactants}} + E_{\text{bulk}}^{\text{reactants}} + \Delta E_{\text{interaction}}^{\text{reactants}} \tag{3}$$

where $E_{\text{reactive}}^{\text{product}}$ and $E_{\text{reactive}}^{\text{reactants}}$ are the energies obtained for the active fragment of product and reactants calculated at higher theoretical level, respectively, and $E_{\text{bulk}}^{\text{product}}$ and $E_{\text{bulk}}^{\text{reactants}}$ denote the energies of the full reaction system of product and reactants calculated at low level. The terms $\Delta E_{\text{interaction}}^{\text{product}}$ and $\Delta E_{\text{interaction}}^{\text{reactants}}$ in Eqs. (2) and (3) are contributions from the overlap between the reactive site and the bulk models for the product and reactants, respectively. If the contributions of these two terms are taken to be approximately equivalent, $\Delta E_{\text{interaction}}^{\text{product}} \approx \Delta E_{\text{interaction}}^{\text{reactants}}$, the exothermic energy can be estimated by using the following equation.

$$E_{\text{exo}} = \left[E_{\text{reactive}}^{\text{product}} - E_{\text{reactive}}^{\text{reactants}}\right] + \left[E_{\text{bulk}}^{\text{product}} - E_{\text{bulk}}^{\text{reactants}}\right] \tag{4}$$

The activation energies, E_a, can be calculated in a similar way.

$$E_a = E_{\text{transition-state}} - E_{\text{reactants}} \tag{5}$$

2.2 ONIOM models

In order to test the performance of the simplified cluster embedding model, both the full QM and two-layered ONIOM calculations are also performed for comparisons. Validation calculations by using the uniform QM level of B3LYP optimizations with effective core potential (LANL2DZ) are only applicable to the reactions on Si(4,4) and Si(5,5) nanotubes, due to the exponential increase in the computational cost with increasing tube diameter. For the validation tests on the other larger SWSiNTs from Si(6,6) to Si(10,10), we resort to the ONIOM models.

The two-level ONIOM(B3LYP/6-31G*: B3LYP/LANL2DZ) model is selected for a direct comparison with the simplified embedding model. Around the reaction center, Cluster I that contains 16 silicon atoms (simplified as Si16 cluster) is used for the high-level treatment method,

while the remaining parts are treated at lower part of B3LYP/LANL2DZ. For Si(4,4) and Si(5,5), both Si16 (Cluster I) and Si30 fragments (Cluster II) are adopted for the high-level core in ONIOM calculations to show the influence of the cluster size on the activation barriers and exothermic energies (Table S2). Some other more economical ONIOM calculations, such as ONIOM(B3LYP/6-31G*: B3LYP/STO-3g) and ONIOM(B3LYP/6-31G*: AM1), are also carried out for comparison. All calculations were performed with the Gaussian03 program [71].

3 Results and discussions

The average bond length of Si–Si bonds in SWSiNTs was found to be 2.268, 2.258, 2.252, 2.249, 2.247, 2.246, and 2.246 Å from Si(4,4) to Si(10,10) at the level of B3LYP/LANL2DZ, respectively, which is almost equal to that of Si–Si bonds of the known disiliranes (2.27–2.33 Å) [72], but slightly shorter than that of surface Si–Si dimeric bonds (2.393 Å) on Si(100) surface at the B3LYP/6-31G* level [73, 74]. The B3LYP/LANL2DZ, fragment embedding (B3LYP/6-31G*: B3LYP/LANL2DZ), and ONIOM ((B3LYP/6-31G*: B3LYP/STO-3g) optimizations were performed to depict possible pathways of dissociative reaction of H_2O on the internal and external sidewalls of SWSiNTs as a function of tube radius. The simplified designations of Int, TS, and Pr are used to represent the intermediate, transition state, and product of dissociative adsorption of H_2O on the sidewalls of SWSiNTs, respectively.

Actually, we also performed the dissociative reaction of H_2O with armchair SiNTs with the unrestricted DFT methods, like what have been done for the understanding of reactions on Si(100) surface [73, 74]. Our calculations at the B3LYP/LANL2DZ level did not display the RHF→UHF instability for wave functions of all intermediates (Int) and transition states (TS). Since the use of multiconfigurational method is necessary to obtain more accurate predictions on the entire potential energy surface, CASSCF(4,4)/6-31G(*d*,*p*) calculations with the two electrons in the π and π^* orbitals of the surface Si dimer and the two electrons in the σ and σ^* orbitals of the dissociative O–H bond in H_2O were also carried out on a truncated model (called Cluster I) of Si(4,4), with the results shown in Figure S1. For the reactions on Si(4,4) tube model, the CASSCF(4,4) treatment for "reactive" center gives similar results to those obtained within the (un)restricted DFT framework (Fig. 2). The restricted wave functions were then employed to investigate the dissociative reaction of H_2O on the sidewalls of SWSiNTs. As shown in Fig. 2 and Figure S1, dissociative reactions of H_2O on both sidewalls of SWSiNTs probably proceed via a concerted pathway. In the following subsections, we will take a closer look at the relative reactivity of water dissociation that is controlled by the curvature and electronic structures of SiNTs (Table 1).

3.1 Internal versus external attack: facial dissociation on the outside

Due to the formidable costs in QM calculations of large-sized nanotubes, the full B3LYP/LANL2DZ optimizations of Int, TS, and Pr stationary points along the dissociation pathway are only feasible for the relatively small tubes, Si(4,4) and Si(5,5), with the calculation results shown in Fig. 2a (for internal sidewall) and Fig. 2b (for external surface), respectively. The dissociative reactions of H_2O on the sidewalls of Si(4,4) and Si(5,5) are initiated by the formation of the stable adsorption intermediate (Int). In the following step, transition state (TS) is reached by overcoming an activation barrier of 25.18 kcal/mol on the internal surface and a relatively lower value of 7.96 kcal/mol on the external site of Si(4,4). Similar results were obtained from the calculations on H_2O@Si(5,5), and the corresponding activation barrier energies are 22.92 and 8.99 kcal/mol on the internal and external surfaces, respectively. Going to the higher theoretical level of CASSCF(4,4)/6-31G(*d*,*p*) for the embedded Cluster I, the activation barriers and exothermic energies of dissociative adsorptions of H_2O on the internal (external) sidewalls of Si(4,4) are 26.90 (10.21) kcal/mol and −8.94 (−25.67) kcal/mol, respectively (Figure S1). This suggests the dissociation of water on the outside of small-diameter SiNTs is easier than that inside of the nanotube. Finally, the dissociative product (**Pr**) is generated, with one hydrogen atom binding with one silicon atom on the surface and the other OH group adsorbing on the neighboring silicon atom. The energies of internal adsorption products are higher than those of Ints by 10.06 and 5.52 kcal/mol for Si(4,4) and Si(5,5), respectively. Such endothermic energies indicate that the internal surface products are thermodynamically unfavorable. In contrast, the external dissociative products are exothermic by 16.07 (on Si(4,4)) and 12.97 (on Si(5,5)) kcal/mol, respectively, indicating that the dissociative reaction of H_2O prefers to proceed on the external surface of SiNT rather than on the internal shell.

The above-mentioned B3LYP/LANL2DZ results on Si(4,4) and Si(5,5) are also useful to test the performance of the simplified multilayer models, in which the active sites are treated with B3LYP/6-31G*, and the rests of SWSiNTs are calculated at the relatively lower level of B3LYP/LANL2DZ. The choice of proper size of the active fragments in such multilevel treatments is crucial to reach a good balance between the computational efficiency and accuracy. Thus, the simplified fragment embedding calculations were performed with the increasingly larger active

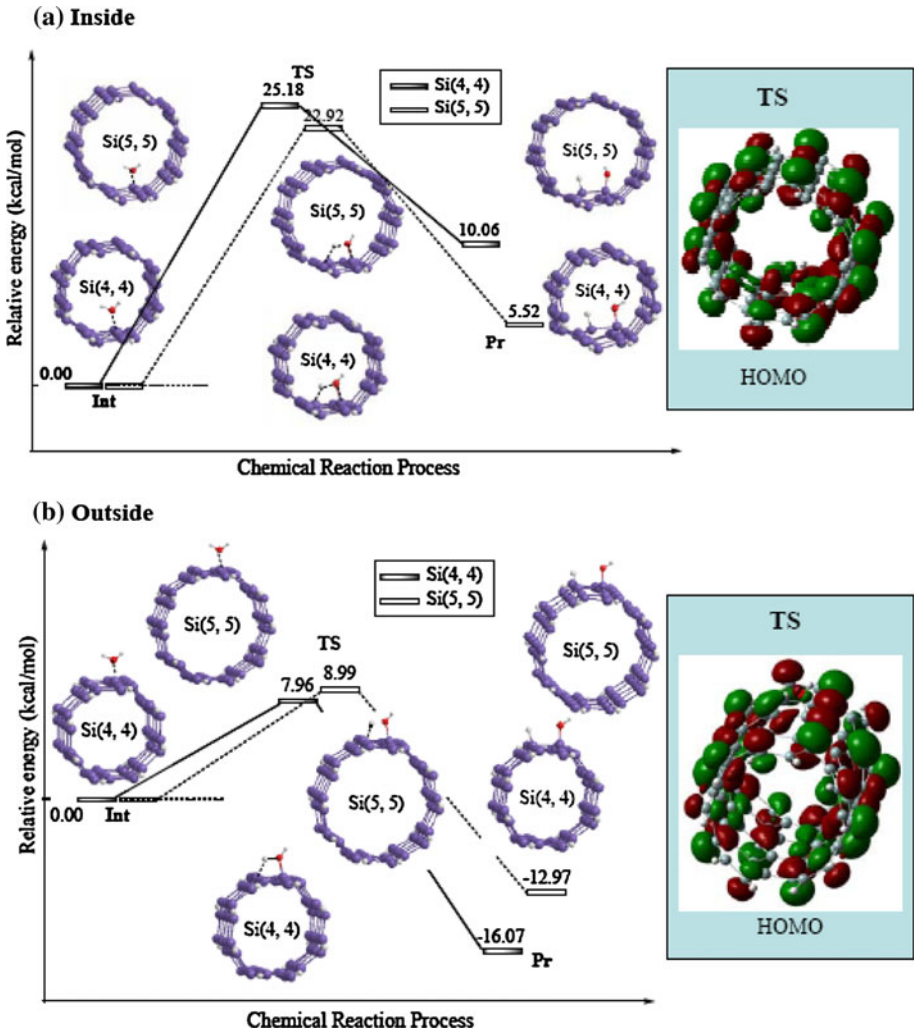

Fig. 2 B3LYP/LANL2DZ optimized geometries of the intermediates (Int), the transition states (TS), and the products (Pr) of dissociative adsorption reactions of H_2O with **a** interior and **b** exterior sidewalls of (4,4) and (5,5) armchair single-walled SiNTs. The frontier orbitals (HOMO, the highest occupied molecular orbital) for transition states are also shown

parts from Cluster I to Cluster III (illustrated in Fig. 1), with the calculated activation barriers and optimized geometry of transition states shown in Fig. 3 and Table S1. As mentioned above, Cluster I model was adopted in both CASSCF(4,4) and B3LYP calculations. These two theoretical levels give similar predictions on the geometries as well as on the energy barriers. For the larger tube, Cluster I may be a little too small to give reasonable predictions, while the calculation results obtained by using Cluster II model are quite close to those come from Cluster III model. The medium-sized active part, like Cluster II, is hence selected for the more time-consuming ONIOM calculations. The calculation results of ONIOM (B3LYP/6-31G*: B3LYP/LANL2DZ) were presented in Table S2, including the optimized geometries and relative energies of stationary points for Si(4,4) and Si(5,5) reaction systems by using Si16 (Cluster I) and Si30 (Cluster II) active clusters, respectively.

To make a better comparison between the simplified fragment embedding and ONIOM models, Fig. 4 displays the concerted dissociative reaction pathways on the sidewalls of Si(4,4) and Si(5,5) obtained by using the different models but the similar active part of Cluster II. Within the simplified fragment embedding model, the transition states (TS) are reached by overcoming activation barriers of 17.69 and 17.45 kcal/mol on the internal surfaces of Si(4,4) and Si(5,5), respectively. In comparison, the ONIOM (B3LYP/6-31G*:B3LYP/LANL2DZ) activation barriers for attachments on internal surfaces are 20.25 kcal/mol and 19.31 kcal/mol, respectively, for Si(4,4) and Si(5,5). The energy barriers obtained from ONIOM are in better agreement with B3LYP/LANL2DZ results than the simplified fragment embedding model. Fortunately, the qualitative trend in relative reactivity and especially the optimized geometry (Fig. 3) and imaginary frequency (Table S3) at transition state is well reproduced by the simplified fragment embedding model. In all **Int**s on the external and internal surfaces, the oxygen atom of H_2O molecule is placed 2.02–2.16 Å away from the SWSiNT sidewalls, and the surface Si–Si bond lengths are found to be 2.34–2.37 Å. The bond lengths are almost identical to those of the normal Si–Si bond length (2.36 Å). At adsorption sites, the bond lengths of Si–Si bonds are a little

Table 1 Selected structural parameters for the transition states (TS) of dissociative adsorption of a single H_2O molecule on the sidewalls of armchair SiNTs

	TS on exterior sidewall (Å)				TS on interior sidewall (Å)			
	Si–Si	Si–O	Si…H	O…H	Si–Si	Si–O	Si…H	O…H
Fragment: Cluster I (B3LYP/6-31G*:B3LYP/LanL2dz)								
Si(4,4)	2.340	1.848	1.836	1.320	2.446	1.856	1.860	1.240
Si(5,5)	2.355	1.844	1.830	1.276	2.412	1.843	1.793	1.289
Si(6,6)	2.354	1.854	1.849	1.279	2.432	1.853	1.831	1.265
Si(7,7)	2.353	1.853	1.846	1.282	2.433	1.852	1.827	1.266
Si(8,8)	2.340	1.853	1.847	1.287	2.420	1.854	1.826	1.271
Si(9,9)	2.343	1.852	1.842	1.288	2.416	1.853	1.825	1.274
Si(10,10)	2.346	1.852	1.842	1.288	2.413	1.853	1.823	1.275
Fragment: Cluster II (B3LYP/6-31G*:B3LYP/LanL2dz)								
Si(4,4)	2.396	1.824	1.831	1.363	2.456	1.857	1.824	1.267
Si(5,5)	2.377	1.829	1.834	1.360	2.447	1.857	1.822	1.269
Si(6,6)	2.364	1.835	1.839	1.339	2.438	1.856	1.822	1.271
Si(7,7)	2.356	1.837	1.844	1.334	2.432	1.856	1.820	1.273
Si(8,8)	2.352	1.840	1.848	1.325	2.427	1.855	1.820	1.275
Si(9,9)	2.349	1.842	1.851	1.318	2.424	1.856	1.819	1.277
Si(10,10)	2.348	1.843	1.853	1.312	2.421	1.855	1.818	1.278
Fragment: Cluster III (B3LYP/6-31G*:B3LYP/LanL2dz)								
Si(4,4)	2.381	1.698	1.617	1.337	2.441	1.856	1.823	1.270
Si(5,5)	2.365	1.839	1.833	1.347	2.438	1.855	1.818	1.274
Si(6,6)	2.358	1.842	1.843	1.329	2.433	1.855	1.817	1.277
Si(7,7)	2.356	1.840	1.848	1.320	2.430	1.854	1.816	1.278
Si(8,8)	2.356	1.850	1.850	1.315	2.427	1.854	1.815	1.280
Si(9,9)	2.366	1.852	1.857	1.288	2.428	1.856	1.819	1.276
Si(10,10)	2.373	1.851	1.839	1.293	2.427	1.855	1.819	1.276
ONIOM (B3LYP/6-31G*: B3LYP/STO-3g)								
Si(4,4)	2.371	1.695	1.684	1.400	2.420	1.866	1.836	1.261
Si(5,5)	2.384	1.818	1.783	1.364	2.418	1.854	1.831	1.266
Si(6,6)	2.379	1.821	1.796	1.356	2.415	1.852	1.826	1.272
Si(7,7)	2.355	1.828	1.838	1.366	2.413	1.851	1.825	1.274
Si(8,8)	2.351	1.830	1.833	1.364	2.410	1.850	1.824	1.277
Si(9,9)	2.348	1.831	1.832	1.361	2.408	1.850	1.823	1.279
Si(10,10)	2.335	1.844	1.822	1.330	2.405	1.850	1.823	1.280
ONIOM (B3LYP/6-31G*: AM1)								
Si(4,4)	2.404	1.692	1.578	2.123	2.400	1.864	1.893	1.225
Si(5,5)	2.443	1.689	1.563	2.213	2.409	1.858	1.872	1.240
Si(6,6)	2.344	1.851	1.844	1.289	2.410	1.855	1.864	1.247
Si(7,7)	2.344	1.853	1.844	1.285	2.409	1.854	1.859	1.251
Si(8,8)	2.340	1.854	1.867	1.280	2.409	1.851	1.855	1.253
Si(9,9)	2.345	1.852	1.846	1.282	2.406	1.853	1.853	1.257
Si(10,10)	2.345	1.851	1.847	1.280	2.405	1.852	1.851	1.259

longer as 2.38–2.40 Å. There is also little geometrical difference in transition states between the external and internal sidewalls of SWSiNTs. The Si–Si distances of TSs are around 2.41 Å, which are approximately 0.02 Å longer than those in Ints. Simultaneously, the Si…O distances in TSs are decreased by 0.19–0.30 Å. Subsequently, the dissociation Pr is generated by the formations of a new Si–O bond and Si–H bond. The Si–O bond lengths in Prs are shortened to about 1.70 Å, and the surface Si–Si bond lengths of SiNT are enlarged to 2.40 Å.

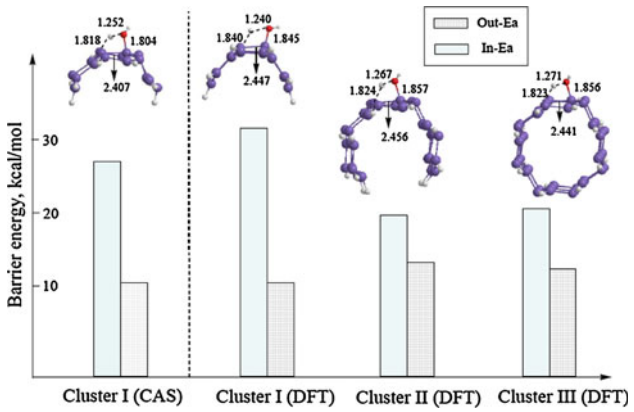

Fig. 3 The influence of the cluster size on the calculated activation energy barriers and the optimized geometry of the transition states within the framework of fragment embedding model

Another advantage of the simplified embedding model is the reduction in computation time in frequency calculation, which is only required for the embedded fragment instead of the whole system (Table S4). This facilitates the further systematic calculations on a series larger reaction systems ranging from Si(5,5) to Si(10,10) using the two-level (B3LYP/6-31G*:B3LYP/LANL2DZ) embedding model. However, ONIOM (B3LYP/6-31G*:B3LYP/LANL2DZ) calculations are still too expensive to cover all the studied systems of up to Si(10,10). Therefore, relatively lower ONIOM models, such as ONIOM(B3LYP/6-31G*:B3LYP/STO-3g) and ONIOM(B3LYP/6-31G*:AM1), were adopted in the following sections. In fact, the ONIOM (B3LYP/6-31G*:B3LYP/STO-3g) results, shown in Figure S2 of Supporting Information, are close to those obtained by the higher ONIOM (B3LYP/6-31G*:B3LYP/LANL2DZ) as well as the simplified embedding model.

3.2 Curvature effects on reactivity of sidewalls

3.2.1 Diameter dependence of binding energies

The binding energy E_b between SiNT and H_2O is obtained from the following expression,

$$E_b = E_{\mathrm{SiNT}} + E_{\mathrm{H_2O}} - E_{\mathrm{SiNT+H_2O}} \quad (6)$$

where the total energy of the SiNT surface absorbing a single H_2O molecule is labeled as $E_{\mathrm{SiNT}} + H_2O$, the energy of SiNT is E_{SiNT}, and the energy of one isolated H_2O is $E_{\mathrm{H_2O}}$.

The calculated binding energies of the H_2O on the internal (In-E_b) and external (Out-E_b) surfaces of SWSiNTs are shown in Fig. 5 and Table S5 as a function of diameters of SWSiNTs at the level of B3LYP/LANL2DZ. As shown in Fig. 5, the internal binding energies decrease slightly from Si(4,4) (5.20 kcal/mol) to Si(10,10) (1.28 kcal/mol) with increasing diameter of the SWSiNTs, while the

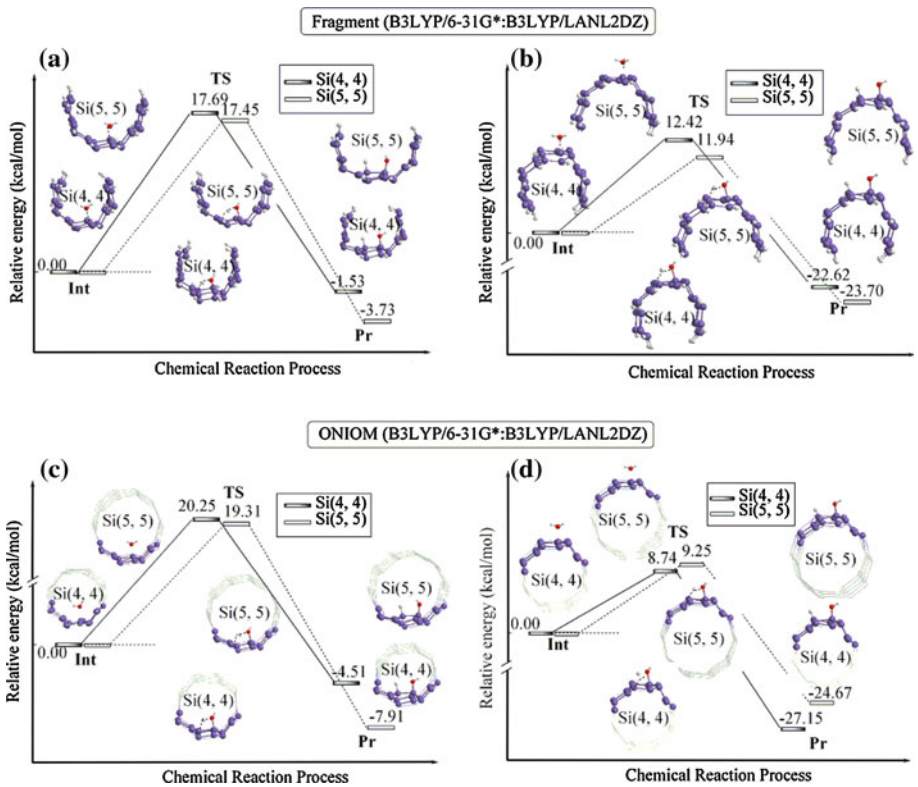

Fig. 4 Optimized geometries of stationary points along the reaction pathway of dissociation of H_2O on the (4,4) and (5,5) armchair single-walled SiNTs by using fragment embedding (**a** for internal and **b** for external reactions) and ONIOM (**c** for internal and **d** for external reactions) models

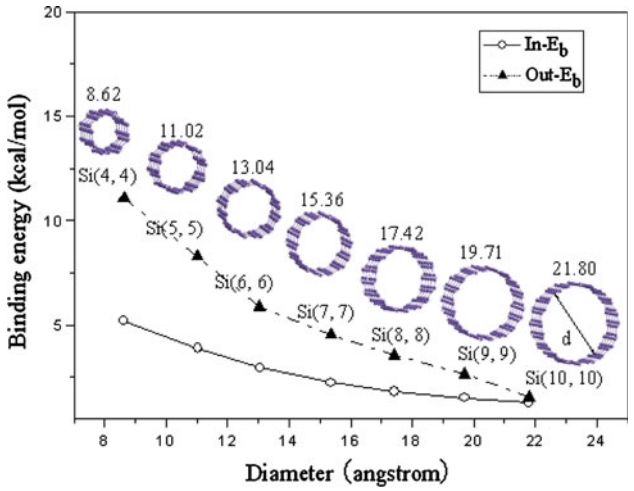

Fig. 5 The binding energies (E_b) between the interior (In) and exterior (Out) surfaces of (n, n) (n = 4–10) SWSiNTs and an absorbed H_2O molecule as a function of the tube diameter, d, (in units of angstrom, shown on the optimized structure) at the level of B3LYP/LanL2dz

external binding energies are decreased more dramatically within a larger range from 11.09 (Si(4,4)) to 1.55 (Si(10,10)) kcal/mol (Table S5).

Similar to the exohedral adsorption of a single atom on the single-walled carbon nanotubes [3, 4, 7], the variation in the binding energy, E_b, of a single water molecule adsorbed on the outer surface of single-walled Si (n,n) follows an expression $E_b = E_0 + C_p/d^p$, where d is the radius of the tube. C_p is a constant that reflects the curvature effect, and the fitted parameter of E_0 represents the extrapolation of binding energy to the limit of adsorption on the planar graphene-like silicon sheet. For the selected H_2O@Si(n, n) systems, the form of $1/d$ (i.e., $p = 1$) gives a better fitting correlation with $E_0 = -4.32$ kcal/mol and $C_1 = 67.51$ Å kcal/mol (correlation coefficient $R^2 = 0.994$) than $1/d^2$ form (in which $p = 2$, $E_0 = 0.71$ kcal/mol, $C_2 = 205.28$ Å^2 kcal/mol, $R^2 = 0.966$). This indicates a very weak interaction between a single water molecule on the planar graphene-like silicon sheet ($d \to \infty$).

3.2.2 *Chemical reactivity*

Figures 6a and 7a show the activation barrier height as a function of the diameters of SWSiNTs. The relative barrier energies are listed in Table S1 (for the simplified fragment embedding model) and Table S6 (ONIOM calculations). It can be seen that the simplified fragment embedding (with Clusters **I**–**III**) and ONIOM models depict the similar pictures, in which the barrier heights of the dissociative adsorption of H_2O on external (out) and internal (in) sidewalls of SWSiNTs just change slightly from Si(5,5) to Si(10,10). The TS is reached by overcoming activation

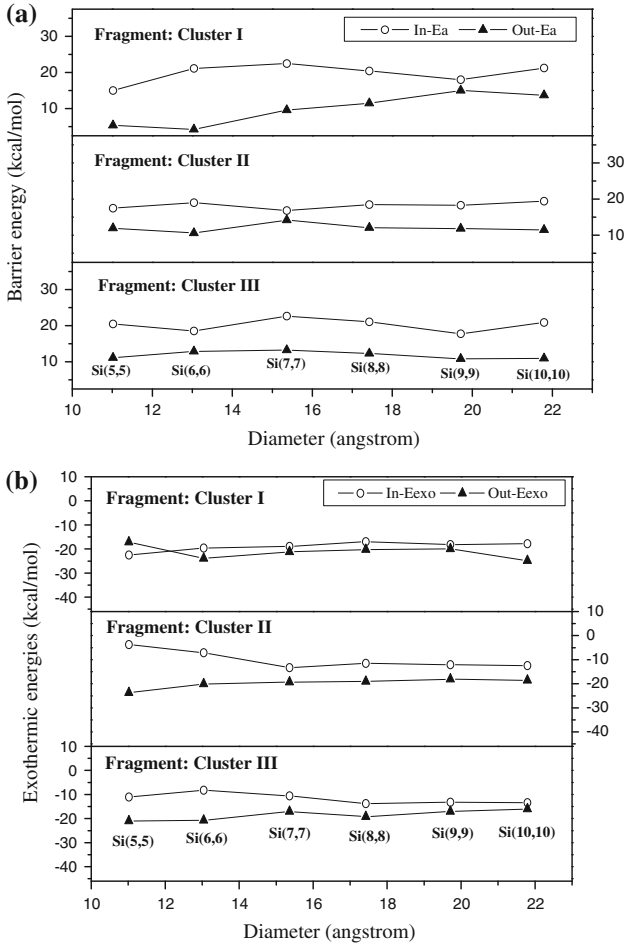

Fig. 6 **a** Activation energy and **b** exothermic energy profiles of dissociative adsorption of H_2O to the exterior (out) and interior (in) sidewalls of (n, n) (n = 5–10) armchair single-walled SiNTs as a function of nanotube diameter, obtained by using the fragment embedding model with the reactive fragment selected as Cluster I, Cluster II, and Cluster III

barrier of around 15–22 kcal/mol on the internal sidewalls and 10–13 kcal/mol on the external sites of SWSiNTs from Si(5,5) to Si(10,10), implying that the dissociative adsorptions of H_2O on the sidewalls of SWSiNTs are facile on external nanotube surfaces. Figures 6b and 7b also show the slight variations in exothermic energies as a function of tube diameters. Despite the weak diameter dependence of exothermic energies for the internal reactions, the increasing magnitude of exothermic energies with increasing diameter implies the stabilization of the internal adsorption products by the larger-sized single-walled silicon nanotube. In contrast, the exothermic energies for the more facial external dissociation almost keep constant around 20 kcal/mol with increasing diameters of nanotubes from Si(5,5) to Si(10,10), similar to those variations in barrier energies.

Such an insensitivity of relative reactivity of dissociations of water on silicon (n, n) nanotube to the surface curvature reminds us of the reactive graphene-like silicon

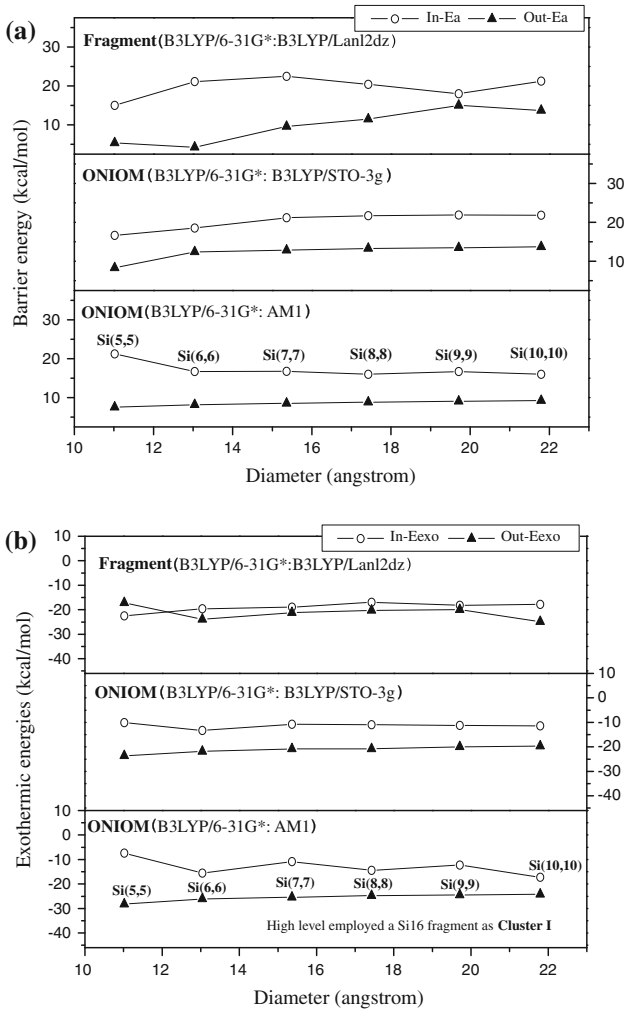

Fig. 7 **a** Activation energy and **b** exothermic energy profiles of dissociative adsorption of H_2O to the exterior (out) and interior (in) sidewalls of (n, n) $(n = 5–10)$ armchair single-walled SiNTs as a function of nanotube diameter obtained by using the fragment embedding and ONIOM models with the reactive part selected as Cluster I

surface toward the attachment of ambient gases. This again indicates the unfavorable sp^2 hybridized silicon framework relative to the sp^3 saturated silicon-containing systems.

4 Conclusions

The dissociative adsorption of H_2O on the sidewalls of (n, n) $(n = 4–10)$ armchair silicon nanotubes (Si(4,4)–Si(10,10)) has been investigated by the multilayered models. In comparison with those B3LYP/LANL2DZ calculations for Si(4,4) and Si(5,5) nanotubes, the simplified fragment embedding and ONIOM methods can give reasonable predictions on the optimized geometries, activation energies, and exothermic energies with the reduced computational costs.

The chemical dissociative adsorptions of H_2O on the external surfaces of armchair SWSiNTs could easily take place with relative lower activation barrier energies (10–13 kcal/mol) than those (15–22 kcal/mol) on the internal surfaces. The adsorption of H_2O molecule on the external surface is thermodynamically favorable with the exothermic energies being around 20 kcal/mol. The autocatalytic behavior of the concerned H_2O/NWSiNT system also deserves our future explorations. Both the activation barriers and exothermic energies are not very sensitive to the increasing diameters of armchair SWSiNTs. It is thus anticipated that the passivation of the outer surface and the removal of water molecules may be crucial for experimental preparation of the single-walled silicon nanotubes.

Acknowledgments This work is supported by the China NSF (No. 20825312), National Basic Research Program (Grant No. 2011CB808600), and the Fok Ying Tong Education Foundation (Grant No. 111013).

References

1. Iijima S (1991) Nature 354:56
2. White CT, Robertson DH, Mintmire JW (1992) Phys Rev B 47:5485
3. Gülseren O, Yildirim T, Ciraci S (2001) Phys Rev Lett 87:116802
4. Gülseren O, Yildirim T, Ciraci S (2002) Phys Rev B 66:121401
5. Tada K, Furuya S, Watanabe K (2001) Phys Rev B 63:155404
6. Niyogi S, Hamon MA, Hu H, Zhao B, Bhowmik P, Sen R, Itkis ME, Haddon RC (2002) Acc Chem Res 35:1105
7. Zhao M, Xia Y, Ma Y, Ying M, Liu X, Mei L (2002) Phys Rev B 66:155403
8. Lu X, Tian F, Xu X, Wang N, Zhang Q (2003) J Am Chem Soc 125:10459
9. Chen ZF, Thiel W, Hirsch A (2003) ChemPhysChem 4:93
10. Ichinohe M, Arai Y, Sekiguchi A, Takagi N, Nagase S (2001) Organometallics 20:4141
11. Nikawa H, Nakahodo T, Tsuchiya T, Wakahara T, Rahman GMA, Akasaka T, Maeda Y, Liu MTH, Meguro A, Kyushin S, Matsumoto H, Mizorogi N, Nagase S (2005) Angew Chem Int Ed 44:7567
12. Sasamori T, Hironaka K, Sugiyama Y, Takagi N, Nagase S, Hosoi Y, Furukawa Y, Tokitoh N (2008) J Am Chem Soc 130:13856
13. Karni M, Apeloig Y, Takagi N, Nagase S (2005) Organometallics 24:6319
14. Kobayashi K, Takagi N, Nagase S (2001) Organometallics 20:234
15. Kobayashi K, Takagi N, Nagase S (1997) Organometallics 16:2489
16. Takeuchi K, Ichinohe M, Sekiguchi A, Guo JD, Nagase S (2009) Organometallics 28:2658
17. Takeuchi K, Ichinohe M, Sekiguchi A, Guo JD, Nagase S (2010) J Phys Org Chem 23:390
18. Kinjo R, Ichinohe M, Seguchi A, Takagi N, Sumimoto M, Nagase S (2007) J Am Chem Soc 129:7766
19. Takagi N, Nagase S (2002) Eur J Inorg Chem 2002:2775
20. Teo BK, Sun XH, Hung TF, Meng XM, Wong NB, Lee ST (2003) Nano Lett 3:1735

21. Wu Y, Cui Y, Huynh L, Barrelet CJ, Bell DC, Lieber CM (2004) Nano Lett 4:433
22. Cui LF, Ruffo R, Chan CK, Peng H, Cui Y (2009) Nano Lett 9:491
23. Gordon MJ, Baron T, Dhalluim F, Gentile P, Ferret P (2009) Nano Lett 9:525
24. Park MH, Kim MG, Joo J, Kim K, Kim J, Ahn S, Cui Y, Cho J (2009) Nano Lett 9:3844
25. Lan J, Cheng D, Cao D, Wang W (2008) J Phys Chem C 112:5598
26. Ma DDD, Lee CS, Au FCK, Tong SY, Lee ST (2003) Science 299:1874
27. Fan R, Wu Y, Li D, Yue M, Majumdar A, Yang P (2003) J Am Chem Soc 125:5254
28. Yang C, Zhong ZH, Lieber CM (2005) Science 310:1304
29. Yang C, Barrelet CJ, Capasso F, Lieber CM (2006) Nano Lett 6:2929
30. Mu C, Zhao Q, Xu DS, Zhuang QK, Shao YH (2007) J Phys Chem B 111:1491
31. Shan Y, Fonash SJ (2008) ACS Nano 2:429
32. Agarwal A, Buddharaju K, Lao IK, Singh N, Balasubramanian N, Kwong DL (2008) Sens Actuators A 145–146:207
33. Tang YH, Pei LZ, Chen YW, Guo C (2005) Phys Rev Lett 95:116102
34. Yang N, Zhang G, Li B (2008) Nano Lett 8:276
35. Hu J, Ouyang M, Yang P, Lieber CM (1999) Nature 399:48
36. Landman U, Barnett RN, Scherbakov AG, Avouris P (2000) Phys Rev B 61:9994
37. Peng Q, Shen J, Chen NX (2008) J Chem Phys 129:034704
38. Wan Y, Sha J, Chen B, Fang Y, Wang Z, Wang Y (2009) Recent Patents Nanotechnol 3:1
39. Park I, Li Z, Pisano A, Williams RS (2010) Nanotechnology 21:015501
40. Zhang RQ, Lee ST, Law CK, Li WK, Teo BK (2002) Chem Phys Lett 364:251
41. Zhang RQ, Lifshitz Y, Lee ST (2003) Adv Mater 15:635
42. Zhang D, Guo G, Liu C, Zhang RQ (2006) J Phys Chem B 110:23633
43. Sha J, Niu J, Ma X, Xu J, Zhang X, Yang Q, Yang D (2002) Adv Mater 14:1219
44. Fagan SB, Mota R, Baierle RJ, Paiva G, da Silva AJR, Fazzio A (2001) J Mol Struct (Theochem) 539:101
45. Solange B, Fagan SB, Baierle RJ, Mota R, da Silva AJR, Fazzio A (2000) Phys Rev B 61:9994
46. Seifert G, Köhler T, Urbassek HM, HernHndez E, Frauenheim T (2001) Phys Rev B 63:193409
47. Andriotis AN, Mpourmpakis G, Froudakis GE, Menon M (2002) New J Phys 4:78
48. Zhang M, Kan YH, Zang QJ, Su ZM, Wang RS (2003) Chem Phys Lett 379:81
49. Bai J, Zeng XC, Tanaka H, Zeng JY (2004) Proc Natl Acad Sci 101:2664
50. Perepichka DF, Rosei F (2006) Small 2:22
51. Pradhan P, Ray AK (2006) J Comput Theor Nanosci 3:128
52. Zhang RQ, Lee HL, Li WK, Li WK, Teo BK (2005) J Phys Chem B 109:8605
53. Yan BH, Zhou G, Wu J, Duan WH, Gu BL (2006) Phys Rev B 73:155432
54. Yan BH, Zhou G, Zeng XC, Wu J, Gu BL, Duan WH (2007) Appl Phys Lett 91:103107
55. Zhao MW, Zhang RQ, Xia YY (2007) J Appl Phys 102:024313
56. Zhao MW, Zhang RQ, Xia YY, Song C, Lee ST (2007) J Phys Chem C 111:1234
57. Zhao MW, Zhu JZ, Xia YY, Lu M (2007) J Phys Chem C 111:2942
58. Zhu WJ, Yan XH, Xiao Y (2008) Phys Lett A 372:1308
59. Maiti A, Andzelm J, Tanpipat N, Allmen PV (2001) Phys Rev Lett 87:155502
60. Kostov MK, Santiso EE, George AM, Gubbins KE, Nardelli MB (2005) Phys Rev Lett 87:136105
61. Warshel A, Levitt M (1976) J Mol Bio 103:227
62. Maseras F, Morokuma K (1995) J Comput Chem 16:1170
63. Shoemaker JR, Burgraff LW, Gordon MS (1999) J Phys Chem A 103:3245
64. Grimley TB, Pisani C (1974) J Phys C 7:2831
65. Pisani C (1978) Phys Rev B 17:3143
66. Ravenek W, Geurts FMM (1986) J Chem Phys 84:1613
67. Fukunishi Y, Nakatsuji H (1992) J Chem Phys 97:6535
68. Whitten JL, Yang H (1996) Surf Sci Rept 24:56
69. Nakatsuji H (1987) J Chem Phys 87:4995
70. Nakatsuji H (1997) Prog Surf Sci 54:1
71. Frisch MJ, Trucks GW, Schlegel HB, Scuseria GE, Robb MA, Cheeseman JR, Montgomery JA Jr, Vreven T, Kudin KN, Burant JC, Millam JM, Iyengar SS, Tomasi J, Barone V, Mennucci B, Cossi M, Scalmani G, Rega N, Petersson GA, Nakatsuji H, Hada M, Ehara M, Toyota K, Fukuda R, Hasegawa J, Ishida M, Nakajima T, Honda Y, Kitao O, Nakai H, Klene M, Li X, Knox JE, Hratchian HP, Cross JB, Adamo C, Jaramillo J, Gomperts R, Stratmann RE, Yazyev O, Austin AJ, Cammi R, Pomelli C, Ochterski JW, Ayala PY, Morokuma K, Voth GA, Salvador P, Dannenberg JJ, Zakrzewski VG, Dapprich S, Daniels AD, Strain MC, Farkas O, Malick DK, Rabuck AD, Raghavachari K, Foresman JB, Ortiz JV, Cui Q, Baboul AG, Clifford S, Cioslowski J, Stefanov BB, Liu G, Liashenko A, Piskorz P, Komaromi I, Martin RL, Fox DJ, Keith T, Al-Laham MA, Peng CY, Nanayakkara A, Challacombe M, Gill PMW, Johnson B, Chen W, Wong MW, Gonzalez C, Pople JA (2003) Gaussian 03, revision D.01. Gaussian, Inc., Pittsburgh, PA
72. Masamune S, Murakami S, Tobita H, Williams DJ (1983) J Am Chem Soc 105:7776
73. Wang Y, Ma J, Inagaki S, Pei Y (2005) J Phys Chem B 109:5199
74. Pei Y, Ma J (2007) J Phys Chem C 111:5486